

Dynamics of electronically phase-separated states in the double exchange model

Jing Luo and Gia-Wei Chern

Department of Physics, University of Virginia, Charlottesville, Virginia 22904, USA (Received 7 January 2020; revised 4 February 2021; accepted 8 February 2021; published 22 March 2021)

We present extensive large-scale dynamical simulations of phase-separated states in the double exchange model. These inhomogeneous electronic states that play a crucial role in the colossal magnetoresistance phenomenon are composed of ferromagnetic metallic clusters embedded in an antiferromagnetic insulating matrix. We compute the dynamical structure factor of these nanoscale textures using an efficient real-space formulation of coupled spin and electron dynamics. Dynamical signatures of the various underlying magnetic structures are identified. At small hole doping, the structure factor exhibits a dominating signal of magnons from the background Néel order and localized modes from magnetic polarons. A low-energy continuum due to large-size ferromagnetic clusters emerges at higher doping levels. Implications for experiments on magnetoresistive manganites are discussed.

DOI: [10.1103/PhysRevB.103.115137](https://doi.org/10.1103/PhysRevB.103.115137)**I. INTRODUCTION**

Phase separation is ubiquitous in systems dominated by nonlinear and nonequilibrium processes [1,2]. In particular, it has been observed in the intermediate state of numerous first-order phase transitions [3]. Nanoscale phase separation also underpins many of the intriguing functionalities of strongly correlated electron materials [4–9]. A prominent example is the colossal magnetoresistance (CMR) phenomenon observed in several manganese oxides [7–11], in which a small change in magnetic field induces an enormous variation of resistance. Detailed microscopic studies have revealed complex nanoscale textures consisting of metallic ferromagnetic clusters embedded in an insulating matrix [12–14]. It is believed that CMR arises from a field-induced percolating transition of the metallic nanoclusters in such mixed-phase states [15–17].

Considerable experimental and theoretical effort has been devoted to understanding the origin of these complex mesoscopic textures in manganites and other correlated systems. An emerging picture is that such inhomogeneous states result from the competition between two distinct electronic phases with nearly degenerate energies [9,10]. Microscopically, the double-exchange interaction [18–20] is considered a major mechanism for electronic phase separation. The double-exchange model describes itinerant electrons interacting with local magnetic moments through the Hund's rule coupling. Since electrons can gain kinetic energy when propagating in a sea of parallel spins, an instability occurs when ferromagnetic domains favored by doped carriers compete with the background antiferromagnetic order. The tendency toward phase separation is further enhanced by factors such as long-range Coulomb interaction, quenched disorder, and coupling to orbital and lattice degrees of freedom [10].

The magnetization dynamics of the hole-doped manganites $L_{1-x}A_x\text{MnO}_3$, where L is a trivalent lanthanide ion and A is a divalent alkaline earth ion, has also been extensively studied

experimentally [21–26]. The majority of the investigations focused on the ferromagnetic phase with optimal hole doping, which is also the regime exhibiting pronounced CMR effect. While the spin-wave spectrum of some ferromagnetic manganites such as $\text{La}_{1-x}\text{Sr}_x\text{MnO}_3$ seems well described by the double-exchange model [27,28], intriguing unconventional magnetic behaviors have also been reported. For example, the spin wave dispersion of manganites with a lower critical temperature is significantly softened near the Brillouin zone boundary. Moreover, the magnon excitations close to zone boundary also exhibit an enhanced broadening. Theoretically, the anomalous spin-wave excitations have been attributed to a host of diverse mechanisms including higher-order effects of spin-charge coupling [29–31], magnon-phonon interaction [32,33], orbital fluctuations [34], and disorder effect [35].

Despite extensive studies on the spin-wave excitations of the ferromagnetic regime, the spin dynamics of the phase-separated states has received much less attention. It remains poorly understood how the resultant spatial inhomogeneity affects the elementary excitations, which intrinsically involve strongly coupled spin and electron degrees of freedom. Important issues such as the spectrum of coupled electron-magnon dynamics in the phase-separated states have yet to be studied theoretically. The difficulty is partly due to the lack of efficient numerical methods. In particular, the absence of translation invariance in a mixed-phase state renders most momentum-based techniques inapplicable. For example, although the magnon spectrum of the ferromagnetic phase has been computed using generalized spin-wave theories that include the electron-spin interaction [27–31], these momentum-based calculations cannot be applied to the phase-separated states of the DE model.

In order to properly account for the spatial inhomogeneity, effective classical or semiclassical spin models, in which the electron degrees of freedom were integrated out beforehand, were employed to compute the magnetic excitation

spectrum [36,37]. However, the subtle interplay between the quantum electron degrees of freedom and the spin dynamics, even treated classical, cannot be captured in such empirical approach. To more properly include the electron effects, an adiabatic dynamical scheme, which integrates out the electrons on the fly of the simulations, have been used to study the dynamical phenomena in inhomogeneous states [38,39]. These approaches, similar to the Born-Oppenheimer approximation in quantum molecular dynamics [40], assume a fast relaxation of the electron gas. Since the electrons are assumed to remain in the instantaneous *equilibrium* states, the adiabatic dynamics not only cannot capture phenomena involving fast electron dynamics but also fails to describe dynamical phenomena with out-of-equilibrium electrons. A detailed discussion of adiabatic versus nonadiabatic spin dynamics, in the context of semiclassical spin-density waves, can be found in Ref. [41]. We also discuss the various dynamical modeling for double-exchange-type models in the Appendix.

In this paper, we present the first large-scale *nonadiabatic* dynamical simulations of the phase-separated states in the single-band double exchange model based on an efficient real-space method for the entangled dynamics of electrons and spins. In our approach, the time evolution of the many-electron wave function, which remains a Slater determinant in double-exchange model, is described by a von Neumann equation for the reduced density matrix, which is coupled to the Landau-Lifshitz dynamics for spins. By starting from various initial states that represent the thermal ensemble of the system, trajectories of spins are obtained by numerically integrating the coupled spin-electron dynamical equations. The dynamical structure factor of the highly inhomogeneous phase-separated states is then computed via the space-time Fourier transform of the spin trajectories. Our results reveal intriguing coexistence of ferromagnetic and antiferromagnetic magnons at large hole doping. Dynamical signatures of magnetic polarons and ferromagnetic metallic clusters are also identified. In particular, an abundance of low-energy magnons is found to arise from the metallic clusters.

The rest of the paper is organized as follows. In Sec. II we discuss the single-band double-exchange (DE) model and its various low temperature phases. Numerical methods used to simulate the equilibrium phases of the DE model are also discussed, with an emphasis on the linear-scaling quantum Langevin dynamics method. We next present in Sec. III our *nonadiabatic* spin-electron dynamics method. In this framework, the evolution of the DE system is governed by the Landau-Lifshitz equation for classical spins, coupled to the von Neumann equation for electron correlation function or reduced density matrix. In Sec. IV, we apply our nonadiabatic dynamics to compute the dynamical structure factor of electronically phase-separated states in the DE model. Analysis of dynamical signatures associated with magnetic polarons, metallic clusters, and background Néel order are also presented. We summarize our work and discuss future applications of our methods in Sec. V. A detailed account of the various dynamical modeling, including the Langevin thermalization method, adiabatic as well as nonadiabatic Landau-Lifshitz dynamics, is given in the Appendix.

II. DOUBLE-EXCHANGE MODEL AND LANGEVIN DYNAMICS

We consider the square-lattice double-exchange (DE) model [18–20], which is one of the most representative models that exhibit spontaneous electronic phase separation. The Hamiltonian of single-band DE model reads

$$\hat{H} = -t \sum_{\langle ij \rangle} (\hat{c}_{i\alpha}^\dagger \hat{c}_{j\alpha} + \text{H.c.}) - J \sum_i \hat{S}_i \cdot \hat{c}_{i\alpha}^\dagger \sigma_{\alpha\beta} \hat{c}_{i\beta}, \quad (1)$$

where repeated indices α, β imply summation. The first term describes the electron hopping: $\hat{c}_{i\alpha}^\dagger$ creates an electron with spin $\alpha = \uparrow, \downarrow$ at site i , $\langle ij \rangle$ indicates the nearest neighbors, t is the electron hopping constant. The second term represents the Hund's rule coupling between electron spin and the local magnetic moments represented by spin operator \hat{S}_i . In order to achieve large-scale simulations, we will use either classical or semiclassical approximation for the local spins.

The equilibrium phases of this square-lattice DE model have been extensively studied theoretically [42–44]. Exactly at half filling, the local spins develop a long-range Néel order in the $T = 0$ insulating ground state. At small electron densities, on the other hand, a metallic state with predominantly ferromagnetic (FM) spin correlation emerges as the ground state. Near half filling with a small hole doping, the FM metal becomes unstable against either a noncollinear magnetic spiral or phase separation [42–45] depending on the strength of the Hund's coupling J . In the large- J regime, the instability of the FM phase leads to phase separation with coexisting FM and Néel domains, as directly verified in Monte Carlo simulations [42].

To obtain the equilibrium phases of the DE system, including the phase-separated states, conventional Monte Carlo simulations are applied to sample the classical spin configurations of the DE Hamiltonian. This is because for a given spin configuration, the DE Hamiltonian, which is quadratic in fermion operators, is essentially a tight-binding model, hence can be exactly solved. For each spin update $\{\mathbf{S}_i\} \rightarrow \{\mathbf{S}'_i\}$, one first computes the free-energy difference $\Delta\mathcal{F} = \mathcal{F}' - \mathcal{F}$, where the free energy for a given spin configuration is obtained by integrating out the electrons

$$\mathcal{F}(\{\mathbf{S}_i\}) = -k_B T \ln \mathcal{Z}_c = -k_B T \ln \text{Tr}_c \exp[-\beta \hat{H}(\{\mathbf{S}_i\})]. \quad (2)$$

Then the Metropolis formula: $P = \min(1, e^{-\Delta\mathcal{F}/k_B T})$ is used to determine whether the proposed spin update is accepted. However, repeated calculation of $\Delta\mathcal{F}$ based on, e.g., exact diagonalization, can be overwhelmingly time consuming. Efficient linear-scaling techniques, such as the kernel-polynomial method (KPM), often have to be used in order to achieve large-scale equilibrium simulations of the DE model [46–48]. However, even with KPM, most local spin-update Monte Carlo methods are not very effective. Here we adopt an efficient adiabatic Langevin dynamics method combined with a gradient extension of the KPM [49–51] to obtain equilibrium phase-separated states. In this approach, the time evolution of the classical spins is governed by the

stochastic model-A dynamics [52]

$$\frac{d\mathbf{S}_i}{dt} = -\alpha \frac{\partial \mathcal{F}}{\partial \mathbf{S}_i} + \xi_i(t) = \alpha \mathbf{T}_i + \xi_i(t), \quad (3)$$

where α is a damping coefficient, and $\xi_i(t)$ is a δ -correlated fluctuating force satisfying $\langle \xi_i(t) \rangle = 0$, and $\langle \xi_i^\mu(t) \xi_j^\nu(t') \rangle = 2\alpha k_B T \delta_{ij} \delta_{\mu\nu} \delta(t - t')$. An implicit Lagrangian multiplier is used to enforce the constant-length constraint $|\mathbf{S}_i(t)| = 1$. Following standard procedure by deriving the associated Fokker-Planck equation, it can be shown that the steady-state configurations are described by the desired Boltzmann distribution.

It should be noted that the Langevin equation (3) describes pure relaxational dynamics of the DE system, which completely ignores the precessional dynamics of spins. In this sense, one cannot apply it to model the general dynamical phenomena. However, for the purpose of sampling spin configurations in equilibrium, the Langevin method is sufficient and very effective, especially compared with the Monte Carlo method. An alternative approach is the quantum version of the stochastic Landau-Lifshitz-Gilbert dynamics [41], which incorporates both precession and relaxation spin dynamics; see Appendix for more details. However, as already noted in the Introduction, such approach is based on the adiabatic approximation. As a result, it cannot be used to describe dynamical process with a timescale shorter than the electron relaxation times.

III. LANDAU-LIFSHITZ VON NEUMANN DYNAMICS

The adiabatic Landau-Lifshitz dynamics, which is similar to the Born-Oppenheimer approximation in quantum molecular dynamics [40], is based on the assumption that the time-scale of electron motion and that of spin dynamics are well separated. Assuming much faster electronic relaxation, the electrons are assumed to remain in equilibrium for any given spin configuration. Consequently, such a dynamical model does not account for the feedback of spin dynamics to the electronic degrees of freedom. More importantly, even without Gilbert damping and stochastic noise, the total energy of the DE system is *not* conserved under the adiabatic Landau-Lifshitz dynamics. The adiabatic approximation is thus inadequate for describing the fundamental entangled dynamics of coupled electron-spin system. We note that adiabatic dynamics for spin-density waves has been formulated in Ref. [41]. Moreover, adiabatic *ab initio* spin dynamics has also been developed based on the adiabatic approximation of the time-dependent density functional theory [53–55].

To go beyond the adiabatic approximation, one needs to treat the electron dynamics on an equal footing with the spin dynamics. Here we present a nonadiabatic dynamics method for the DE system, which is similar in spirit to the Ehrenfest method in quantum molecular dynamics simulations [40,56,57]. We assume that the quantum state of the DE system is a direct product state: $|\Omega(t)\rangle = |\Phi(t)\rangle \otimes |\Psi(t)\rangle$, where $|\Phi\rangle$ and $|\Psi\rangle$ denote the spin and electron wave functions, respectively. Consistent with the classical approximation for spins, we assume $|\Phi\rangle$ is a direct product of single-site spin state: $|\Phi(t)\rangle = \prod_i |\phi_i(t)\rangle$. This is equivalent to a mean-field approximation for the quantum spins. We then

define time-dependent local moment $\mathbf{S}_i(t) = \langle \phi_i(t) | \hat{\mathbf{S}}_i | \phi_i(t) \rangle$ as the expectation value of the spin operator.

By tracing out the spin degrees of freedom, the evolution of the electron wave function $|\Psi(t)\rangle$ is described by the Schrödinger equation with a time-varying DE Hamiltonian

$$i\hbar \frac{d|\Psi(t)\rangle}{dt} = \hat{\mathcal{H}}_e(\{\mathbf{S}_i(t)\}) |\Psi(t)\rangle, \quad (4)$$

where the effective electron Hamiltonian is defined as

$$\hat{\mathcal{H}}_e(\{\mathbf{S}_i\}) = \langle \Phi(t) | \hat{\mathcal{H}} | \Phi(t) \rangle, \quad (5)$$

and $\hat{\mathcal{H}}$ is the DE Hamiltonian in Eq. (1). Next, to derive the spin dynamics, we switch to the Heisenberg picture. The equation of motion for vector $\mathbf{S}_i(t)$ is then

$$\frac{d\mathbf{S}_i}{dt} = \frac{i}{\hbar} [\hat{\mathcal{H}}, \hat{\mathbf{S}}_i], \quad (6)$$

where $\langle \dots \rangle$ means expectation value computed using the full quantum state $|\Omega\rangle$. Using the product nature of the spin state $|\Phi\rangle$, the above equation can be expressed as the standard Landau-Lifshitz (LL) equation

$$\frac{d\mathbf{S}_i}{dt} = \mathbf{S}_i \times \frac{\partial \mathcal{E}}{\partial \mathbf{S}_i}, \quad (7)$$

where the effective energy is

$$\mathcal{E}(\{\mathbf{S}_i\}) = \langle \Psi(t) | \hat{\mathcal{H}}_e | \Psi(t) \rangle. \quad (8)$$

It is worth noting that the equivalence between Landau-Lifshitz dynamics and the mean-field type approximation for quantum spin dynamics has been pointed out in earlier works [58,59]. Since the linearized Landau-Lifshitz equation is equivalent to the leading-order Holstein-Primarkoff expansion, the above treatment can also be viewed as a semiclassical dynamics for quantum spins in the DE model. We also note that classical spin approximation is widely used in the study of CMR phenomena. Our approach here thus corresponds to the dynamical generalization of the classical picture used for DE-type systems.

Substituting the explicit form of the DE Hamiltonian Eq. (1) into the above Landau-Lifshitz equation, we obtain

$$\frac{d\mathbf{S}_i}{dt} = -J\mathbf{S}_i \times \sigma_{\alpha\beta} \rho_{i\beta, i\alpha}(t). \quad (9)$$

Here we have defined the time-dependent single-electron density matrix or correlation function

$$\rho_{i\alpha, j\beta}(t) \equiv \langle \Psi(t) | \hat{c}_{j\beta}^\dagger \hat{c}_{i\alpha} | \Psi(t) \rangle. \quad (10)$$

Since the DE Hamiltonian is bilinear in fermion operators, the many-electron wave function $|\Psi(t)\rangle$ remains a single Slater-determinant state if it is a pure state initially. However, the integration of the Slater determinant is rather cumbersome numerically and has only been used for rather small size simulations [60,61].

Instead of evolving the Slater determinant wave function, one could equally describe the electron dynamics in terms of the reduced density matrix based on the Heisenberg picture. An additional advantage of this formulation is that it can account for the initially mixed quantum states. Details of the generalization to include the ensemble average of the initial states can be found in the Appendix. To describe the electron

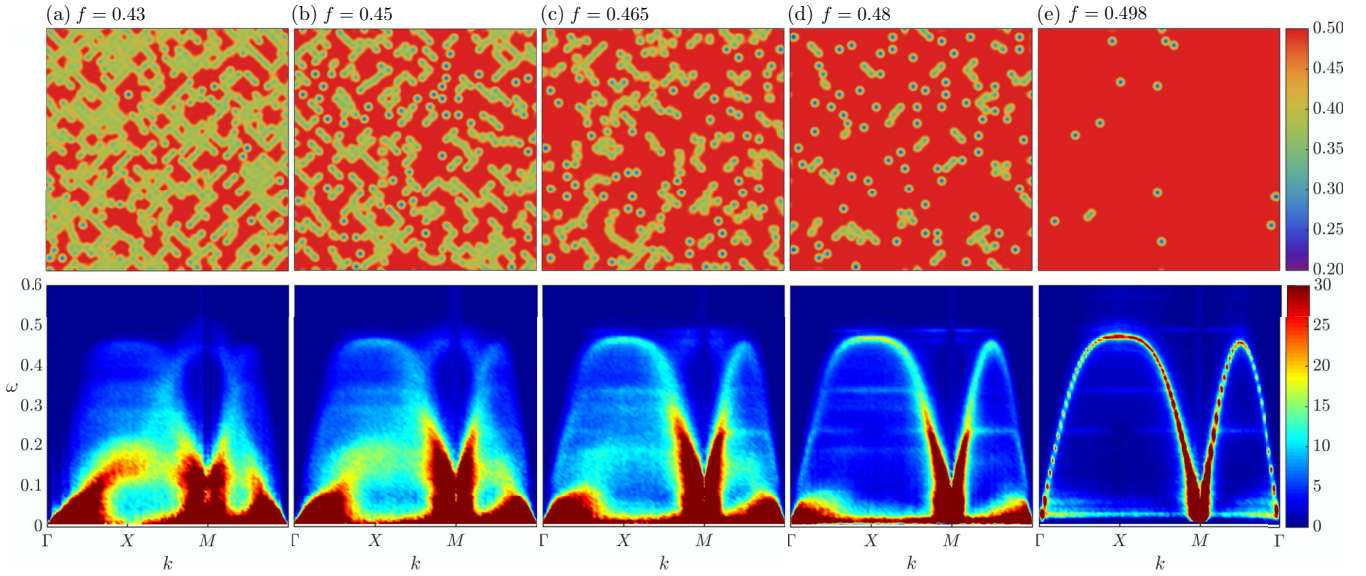


FIG. 1. Upper panels: density plots of the onsite electron number $n(\mathbf{r}_i) = \langle \hat{c}_{i,\alpha}^\dagger \hat{c}_{i,\alpha} \rangle$ in sample phase-separated states for varying electron filling fraction $f = \sum_i n(\mathbf{r}_i)/2N$, where N is the number of lattice sites, obtained from Langevin dynamics simulations on a 60×60 lattice with Hund's coupling $J = 6t$ and temperature $T = 5 \times 10^{-4}t$. The corresponding dynamical structure factors $S(\mathbf{q}, \omega)$ averaged over tens of independent initial states are shown in the lower panels. The high-symmetry points of the Brillouin zone are $\Gamma = (0, 0)$, $X = (\pi, 0)$, $M = (\pi, \pi)$.

dynamics in our formalism, we define a time-dependent “first-quantization” Hamiltonian matrix

$$H_{i\alpha,j\beta} = -t_{ij}\delta_{\alpha\beta} - \mathbf{J}\mathbf{S}_i \cdot \boldsymbol{\sigma}_{\alpha\beta} \delta_{ij}. \quad (11)$$

The DE model in Eq. (1) can then be expressed as

$$\hat{\mathcal{H}} = \sum_{i,j} \sum_{\alpha,\beta} H_{i\alpha,j\beta} \hat{c}_{i\alpha}^\dagger \hat{c}_{j\beta}. \quad (12)$$

In terms of matrix H , the reduced density matrix satisfies the von Neumann equation

$$\frac{d\rho}{dt} = i[\rho, H]. \quad (13)$$

Substituting Eq. (11) for H to the above equation yields

$$\begin{aligned} \frac{d\rho_{i\alpha,j\beta}}{dt} &= i(t_{ik} \rho_{k\alpha,j\beta} - \rho_{i\alpha,k\beta} t_{kj}) \\ &+ i\mathbf{J}(\mathbf{S}_i \cdot \boldsymbol{\sigma}_{\alpha\gamma} \rho_{i\gamma,j\beta} - \rho_{i\alpha,j\gamma} \boldsymbol{\sigma}_{\gamma\beta} \cdot \mathbf{S}_j). \end{aligned} \quad (14)$$

It can be readily verified that the total energy of the system $E = \langle \mathcal{H} \rangle = \text{Tr}(\rho H)$ is a constant of motion. The numerical efficiency of integrating the von Neumann equation can be improved with optimized sparse-matrix multiplication algorithms. A similar formulation has been developed for the semiclassical dynamics of spin density waves in the Hubbard model [41].

IV. DYNAMICAL STRUCTURE FACTOR OF PHASE-SEPARATED STATES

To compute the dynamical structure factor of the phase-separated states, the initial state is prepared using the KPM Langevin simulations at a temperature of $T = 5 \times 10^{-4}t$. A few examples of such mixed-phase states on a 60×60 square lattice are shown in the upper panels of Fig. 1. The red region

corresponds to the half-filled insulating background with the antiferromagnetic order, while the green and blue regions indicate metallic FM domains with low electron density. Interestingly, in addition to forming the FM puddles, a fraction of the doped holes are self-trapped in a composite object which can be viewed as the magnetic analog of polaron [62–65].

For each of the initial configurations prepared by the Langevin simulations, a fourth-order Runge-Kutta method is used to integrate the nonadiabatic Landau-Lifshitz-von Neumann equations, i.e., Eqs. (9) and (A27). From the numerically obtained spin trajectories $\mathbf{S}_i(t)$, we compute the dynamical correlation function

$$\mathcal{S}(\mathbf{q}, t) = \langle \mathbf{S}_{\mathbf{q}}(t) \cdot \mathbf{S}_{\mathbf{q}}^*(0) \rangle, \quad (15)$$

where $\mathbf{S}_{\mathbf{q}}(t) \equiv \sum_i \mathbf{S}_i(t) \exp(i\mathbf{q} \cdot \mathbf{r}_i) / \sqrt{N}$ is the spatial Fourier transform of the instantaneous spin configuration, and $\langle \dots \rangle$ denotes the ensemble average over independent initial states of a given temperature. The dynamical structure factor is then given by

$$\begin{aligned} \mathcal{S}(\mathbf{q}, \omega) &= \int \mathcal{S}(\mathbf{q}, t) e^{-i\omega t} dt \\ &= \frac{1}{N} \sum_{ij} \int dt \langle \mathbf{S}_i(t) \cdot \mathbf{S}_j(0) \rangle e^{-i\omega t}, \end{aligned} \quad (16)$$

which is essentially the space-time Fourier transform of the spin-spin correlator $C(\mathbf{r}_{ij}, t) = \langle \mathbf{S}_i(t) \cdot \mathbf{S}_j(0) \rangle$. Importantly, the dynamical simulation here is completely deterministic and energy conserving. The lower panels of Fig. 1 show the $\mathcal{S}(\mathbf{q}, \omega)$ of phase-separated states with five different electron filling fractions; each is averaged over 50 distinct initial states.

Since the Néel order parameter, characterized by the wave vector $\mathbf{Q} = (\pi, \pi)$ at the M point, is not a conserved

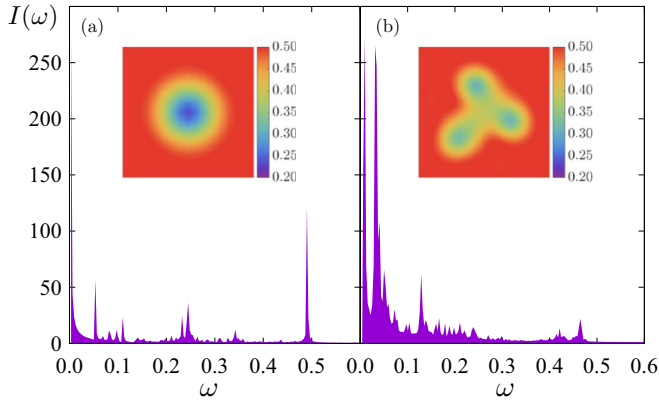


FIG. 2. The power spectrum $I(\omega) = \sum_{i \in C} |\tilde{\mathbf{S}}_i(\omega)|^2$ of (a) a magnetic polaron and (b) a FM metallic cluster consisting of roughly 20 spins. Here the sum runs over spins in the FM domain of these object. The inset shows the electron density plot $n(\mathbf{r}_i) = \langle c_{i\alpha}^\dagger c_{i\alpha} \rangle$. With a large Hund's coupling $J = 6t$, the size of the magnetic polaron is rather small, with a radius of roughly three lattice constants.

quantity, the fluctuations of the associated Fourier component $\tilde{\mathbf{S}}(\mathbf{Q}, t) \equiv \sum_i \mathbf{S}_i(t) e^{i\mathbf{Q}\cdot\mathbf{r}_i}$ produce a huge artifact in the raw data of the dynamical structure factor. Interestingly, we found that the drifting of this Goldstone mode of finite lattices exhibits a $1/\omega$ power-law behavior, extending to very high energies. This observation thus allows us to systematically remove the large artificial signal in the vicinity of the M point. The $\mathcal{S}(\mathbf{q}, \omega)$ shown in Fig. 1 were obtained after this subtraction.

The dynamical structure factor in the vicinity of half filling is dominated by the background antiferromagnetic spin-wave excitations, as shown in Fig. 1(e). The pronounced signals around the M point correspond to the Goldstone modes of the underlying Néel order. As mentioned above, the doped holes in this regime are localized by the self-induced potential in a magnetic polaron. Numerically, each polaron is found to accommodate nearly exactly one hole. To understand the nature of the associated spin excitations, we focus on the dynamics of a single magnetic polaron. We first perform relaxational dynamics on a perturbed half-filled Néel state (by flipping a center spin) with exactly one electron removed to obtain the initial states. From the spin dynamics, we compute the power spectrum $I(\omega) \equiv \sum_{i \in C} |\tilde{\mathbf{S}}_i(\omega)|^2$, where $\tilde{\mathbf{S}}_i(\omega) = \int \mathbf{S}_i(t) e^{-i\omega t} dt$ and the summation is over five spins at the center of the polaron. The computed spectrum, shown in Fig. 2(a), is characterized by prominent peaks at, e.g., $\omega/t = 0.05, 0.25, 0.49$, corresponding to eigenenergies of the spin-wave excitations localized at the magnetic polaron. Importantly, these localized magnons contribute to the flat bands seen in $\mathcal{S}(\mathbf{q}, \omega)$.

With increasing hole doping, the antiferromagnetic spin-wave dispersion is still visible, yet with gradually reduced strength. Some of the flat bands due to magnetic polarons also persist. An intriguing new feature is the emergence of a continuum of low-energy magnons throughout the whole Brillouin zone. It is tempting to associate this continuum with the metallic FM clusters whose size also grows with increasing hole doping; see Fig. 1. To this end, we examine the spectrum

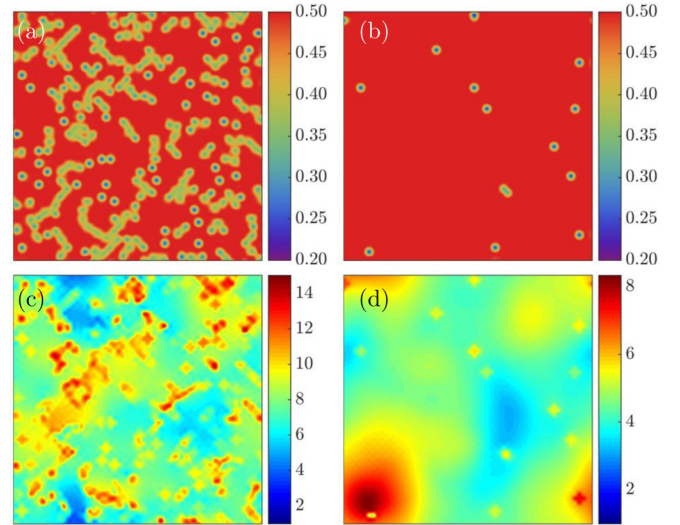


FIG. 3. Top panels show the density plot $n(\mathbf{r}_i) = \langle c_{i\alpha}^\dagger c_{i\alpha} \rangle$ of one particular phase-separated state for filling fractions (a) $f = 0.465$ and (b) $f = 0.498$. The simulated system size is 60×60 . The corresponding spatial profile of spin excitations $\mathcal{F}(\mathbf{r}_i) = \int_{\omega_1}^{\omega_2} |\tilde{\mathbf{S}}_i(\omega)|^2 d\omega$ is shown in panels (c) and (d), respectively, where $\omega_1 = 0.006283$ and $\omega_2 = 0.09425$.

of metallic clusters of varying shapes and sizes. Similar to the preparation of the magnetic polaron, we manually create such structures by carefully tuning the hole doping with the cluster size. Figure 2(b) shows the $I(\omega)$ of a sample cluster consisting of roughly 20 spins. A few pronounced peaks, corresponding to the dominant quantized magnons, can be seen in the spectrum. While the intensity and position of these peaks depend on the geometric details of the FM clusters, a common feature of the cluster spectrum is the appearance of numerous low energy modes.

To further investigate the nature of these low-energy magnons, we compare their spatial profile $\mathcal{F}(\mathbf{r})$ with the corresponding electron density plot $n(\mathbf{r})$ for a particular initial state, as demonstrated in Fig. 3 for two electron filling fractions. Here the magnon profile function is defined as the integral of the spin Fourier components $\mathcal{F}(\mathbf{r}_i) = \int_{\omega_1}^{\omega_2} |\tilde{\mathbf{S}}_i(\omega)|^2 d\omega$ over a finite band $[\omega_1, \omega_2]$ of small energies. In the case of electron filling $n = 0.465$, where the system is spontaneously segregated into FM domains of various sizes in an AFM background, the dominant spin excitations in this energy range are from the FM clusters of the doped holes; see Figs. 3(a) and 3(c). For even smaller hole doping with $f = 0.498$, the intensity plot of $\mathcal{F}(\mathbf{r})$ exhibits a complex long-wavelength pattern of the Néel background as shown in Fig. 3(d). Distinctive signals can be seen that are contributed from the small-size magnetic polarons.

We next examine the spectral distribution of low-energy spin excitations of the phase-separated states. Figure 4(a) shows the log-log plot of the dynamical structure factor $\mathcal{S}(\mathbf{q}, \omega)$ versus ω at a few selected wave vectors. Each curve is again obtained after averaging over tens of different mixed-phase configurations. These distributions exhibit an abrupt drop above a band edge $E_b \sim 0.5t$, indicating the absence of magnon density of states at high energies; see also the density

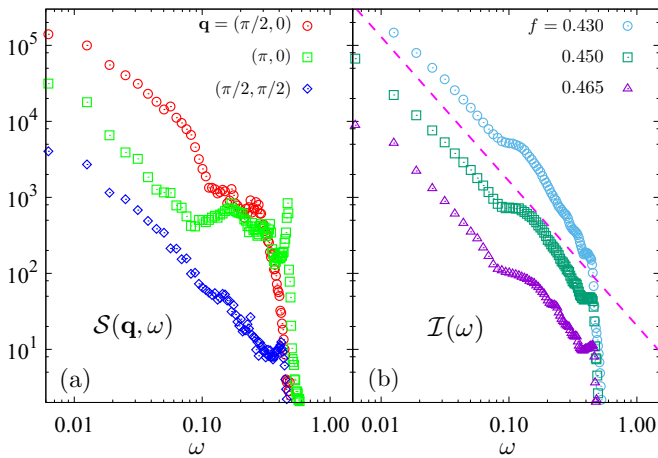


FIG. 4. (a) The dynamical structure factor $S(\mathbf{q}, \omega)$ versus ω at a few selected wavevectors \mathbf{q} for filling fraction $f = 0.465$. (b) The frequency dependence of the spin excitation spectrum $\mathcal{I}(\omega) \equiv \sum_{\mathbf{q}} S(\mathbf{q}, \omega)/N$ integrated over the whole Brillouin zone, at varying electron filling fractions. The curves are shifted vertically for clarity. The dashed line shows the $\omega^{-2.1}$ power-law dependence.

plots in Fig. 1. While the dynamical structure factor at the three different \mathbf{q} 's shows rather distinct ω dependences at high energies, a pronounced increase of $S(\mathbf{q}, \omega)$ at small ω can be seen for all three wave vectors shown in Fig. 4(a).

The overall density of states (DOS) of the low-energy magnons can be inferred from the spectral function $\mathcal{I}(\omega) = \sum_{\mathbf{q}} S(\mathbf{q}, \omega)/N$, which is the dynamical structure factor averaged over the whole Brillouin zone. Figure 4(b) shows the log-log plots of the numerical spectral function $\mathcal{I}(\omega)$ for three different filling fractions. Interestingly, they show strong similarities with each other, especially with increasing hole doping. At high energies, one can see a clear band edge and a shoulderlike feature. The distribution functions $\mathcal{I}(\omega)$ develop a sharp peak at $\omega \rightarrow 0$, which indicates a significant increase in the magnon DOS at small ω . The nearly linear segments in the log-log plot of Fig. 4(b) suggest a power-law behavior. It is worth noting that a similar disorder-induced peak at $\omega \rightarrow 0$ also appears in the magnon DOS in different localized spin models [66,67].

In our case, these low-energy magnons can be viewed as descending from the zero-energy modes of individual isolated FM clusters. These zero modes acquire a finite energy through coupling to the Néel background. For short-range spin-spin interactions, this energy shift of the zero modes is expected to scale as the circumference of the FM cluster. Since the electron-mediated spin interactions are long ranged, the energy shift might scale differently. For simplicity, we assume a power-law relation $\omega \sim s^{1/\Delta}$ between the acquired energy ω of the zero mode and the size s of the FM puddle. For example, $\Delta = 2$ corresponds to the case $\omega \sim \ell$, where ℓ is the linear cluster size. The density of states $\rho(\omega)$ is then related to the distribution of s through $\rho(\omega) \sim n(s) \omega^{\Delta-1}$. In the vicinity of the cluster percolation transition, one expects a power-law cluster-size distribution $n(s) \sim 1/s^\tau$ for large clusters; here τ is the Fisher's exponent [68]. This in turn indicates a power-law DOS $\rho(\omega) \sim 1/\omega^{\Delta(\tau-1)+1}$. Numerically, we find that Δ is very close to 1 [69].

V. SUMMARY AND OUTLOOK

To summarize, we have presented an efficient numerical framework for the real-space dynamical simulation of the double-exchange model. Focusing on the regime with small hole doping, we compute the dynamical structure factor of the electronically phase-separated states. In particular, we found an emerging low-energy magnon continuum that is attributed to the quasi-zero-modes of large-size metallic FM clusters. Such abundance of low-energy magnons has been observed in recent neutron-scattering measurement of ferromagnetic manganites $\text{La}_{0.7}\text{Ca}_{0.3}\text{MnO}_3$ close to optimal doping [26]. We have also observed the coexistence of FM and AFM magnons in the dynamical structure factor with larger hole doping, a result consistent with recent experiment [70]. Our work thus opens an avenue for dynamical simulations of electronic inhomogeneous states in other systems.

It is worth pointing out that magnon spectrum in real materials also depends on factors such as long-range dipole-dipole or Coulomb interactions, anisotropy, charge-phonon, and charge-orbital coupling. Our goal here is to examine the intrinsic effects of phase separation on the coupled electron-spin dynamics. While several mechanisms, such as magnon-phonon interaction [32,33], orbital fluctuations [34], and disorder effect [35], have been proposed to explain the unusual softening and broadening of spin waves in some manganites, recent experiment [26] highlighted the possibility that this anomalous behavior could be simply caused by the electronic phase separation. With our efficient formulation, it is now possible to quantitatively study the FM magnons in the mixed-phase state, which will be left for future study.

ACKNOWLEDGMENTS

We thank Kipton Barros for the help with the kernel polynomial method. This work is partially supported by the Center for Materials Theory as a part of the Computational Materials Science (CMS) program, funded by the U.S. Department of Energy, Office of Science, Basic Energy Sciences, Materials Sciences and Engineering Division. The authors also acknowledge the support of Advanced Research Computing Services at the University of Virginia.

APPENDIX: DYNAMICAL MODELING FOR DOUBLE-EXCHANGE SYSTEMS

Most numerical investigations of the double-exchange (DE) systems [18–20] have so far focused on their equilibrium properties. In particular, extensive Monte Carlo simulations and dynamical mean-field theory calculations have been used to obtain the phase diagrams. However, dynamical simulations of inhomogeneous phases in DE models have yet to be explored. In this Appendix, we discuss the various dynamics of the double-exchange (DE) system and their numerical formulations. We first review the adiabatic spin dynamics, which is analogous to the Born-Oppenheimer approximation in quantum molecular dynamics simulations [40]. Next we discuss the nonadiabatic Ehrenfest dynamics for coupled electron-spin systems. Finally we present details of the

Landau-Lifshitz-von Neumann method for the nonadiabatic dynamics of the DE system.

1. Adiabatic spin dynamics

In the adiabatic approximation, which is similar to Born-Openheimer approximation for quantum molecular dynamics [40], electrons are assumed to quickly relax to the equilibrium state corresponding to the instantaneous spin configuration $\{\mathbf{S}_i\}$. One can thus define an effective energy functional for the spins by integrating out electrons

$$\mathcal{F}(\{\mathbf{S}_i\}) = -k_B T \ln \mathcal{Z}_c \equiv -k_B T \ln \text{Tr}_c(e^{-\beta \mathcal{H}}), \quad (\text{A1})$$

which is essentially the canonical free energy of the electrons. Here $\beta = 1/k_B T$ is the inverse temperature, and we have also defined the electron partition function \mathcal{Z}_c . This free energy can also be written as

$$\mathcal{F} = \mathcal{E} - T \mathcal{S}, \quad (\text{A2})$$

where \mathcal{E} is the internal energy

$$\mathcal{E} = \langle \mathcal{H} \rangle = \frac{1}{\mathcal{Z}_c} \text{Tr}_c(e^{-\beta \mathcal{H}} \mathcal{H}), \quad (\text{A3})$$

and \mathcal{S} is the entropy of the electron system. In terms of the eigenenergies $\varepsilon_m = \varepsilon_m(\{\mathbf{S}_i\})$, which are functions of the instantaneous spin configuration, the electron energy and entropy can be expressed as

$$\mathcal{E} = \sum_m \varepsilon_m f_m, \quad (\text{A4})$$

$$\mathcal{S} = -k_B \sum_m [f_m \ln f_m + (1 - f_m) \ln(1 - f_m)], \quad (\text{A5})$$

where $f_m = 1/(\exp(\beta \varepsilon_m) + 1)$ is the Fermi-Dirac function for the electron occupation. For simplicity, here we have set the zero of the electron energy to be the chemical potential.

Given this effective spin energy \mathcal{F} , the torques acting on spins can be defined as

$$\mathbf{T}_i = -\frac{\partial \mathcal{F}}{\partial \mathbf{S}_i}. \quad (\text{A6})$$

This torque can also be thought of as an effective local exchange field, which plays a central role in spin dynamics. For example, the pure relaxational dynamics, or model A [52], is described by the following stochastic equation

$$\frac{d\mathbf{S}_i}{dt} = -\alpha \frac{\partial \mathcal{F}}{\partial \mathbf{S}_i} + \boldsymbol{\xi}_i(t) = \alpha \mathbf{T}_i + \boldsymbol{\xi}_i(t), \quad (\text{A7})$$

where α is a damping coefficient, and $\boldsymbol{\xi}_i(t)$ is a δ -correlated fluctuating force satisfying

$$\langle \boldsymbol{\xi}_i(t) \rangle = 0, \quad \langle \xi_i^\mu(t) \xi_j^\nu(t') \rangle = 2\alpha k_B T \delta_{ij} \delta_{\mu\nu} \delta(t - t'). \quad (\text{A8})$$

An implicit Lagrangian multiplier is used to enforce the constraint $|\mathbf{S}_i(t)| = 1$. This equation can also be viewed as the Langevin dynamics of the spins [49,50], which has proven a powerful method for simulating equilibrium phases of the DE systems. More generally, the spin dynamics is described by the stochastic Landau-Lifshitz or Landau-Lifshitz-Gilbert (LLG) equation [71–73]

$$\frac{d\mathbf{S}_i}{dt} = -\mathbf{S}_i \times (\mathbf{T}_i + \boldsymbol{\xi}_i) - \alpha \mathbf{S}_i \times (\mathbf{S}_i \times \mathbf{T}_i). \quad (\text{A9})$$

Here the first term on the right hand side describes the energy-conserving precessional dynamics of spins, while the second term represents the dissipation effect. This stochastic LLG equation can be used to simulate both equilibrium or nonequilibrium magnetic dynamical phenomena. However, it should be noted that electrons are assumed to be in quasiequilibrium state within the adiabatic approximation.

The most time-consuming part of such adiabatic dynamical simulations, either the relaxational or the LLG dynamics, is the computation of the torque in Eq. (A6) due to itinerant electrons. Using Eqs. (A2) and (A4) for the electron free energy and internal energy, respectively, the derivative of \mathcal{F} is given by

$$\frac{\partial \mathcal{F}}{\partial \mathbf{S}_i} = \sum_m f_m \frac{\partial \varepsilon_m}{\partial \mathbf{S}_i} + \sum_m \varepsilon_m \frac{\partial f_m}{\partial \mathbf{S}_i} - T \frac{\partial \mathcal{S}}{\partial \mathbf{S}_i}.$$

Using Eq. (A5) for the electron entropy, it can be shown after some algebra that the last two terms in the above expression cancel each other. This can also be derived directly from the free-energy expression

$$\mathcal{F} = -k_B T \sum_m (1 + e^{-\beta \varepsilon_m}). \quad (\text{A10})$$

Taking the derivative with respect to spin, we have

$$\begin{aligned} \frac{\partial \mathcal{F}}{\partial \mathbf{S}_i} &= -k_B T \sum_m \frac{e^{-\beta \varepsilon_m}}{1 + e^{-\beta \varepsilon_m}} \frac{\partial(-\beta \varepsilon_m)}{\partial \mathbf{S}_i} \\ &= \sum_m f_m \frac{\partial \varepsilon_m}{\partial \mathbf{S}_i}. \end{aligned} \quad (\text{A11})$$

A similar result has been obtained previously in the context of quantum molecular dynamics [74,75]. To further simplify this expression, we write the electron Hamiltonian in terms of quasiparticle number operators: $\mathcal{H} = \sum_m \varepsilon_m \hat{n}_m$, where the eigenenergies depend on the instantaneous spin configuration $\varepsilon_m = \varepsilon_m(\{\mathbf{S}_i(t)\})$. We thus have

$$\frac{\partial \hat{\mathcal{H}}}{\partial \mathbf{S}_i} = \sum_m \hat{n}_m \frac{\partial \varepsilon_m}{\partial \mathbf{S}_i}. \quad (\text{A12})$$

Next we average over the electrons and use the identity $\langle \hat{n}_m \rangle = f_m$. We then obtain a generalization of the Hellmann-Feynman theorem

$$\mathbf{T}_i = -\left\langle \frac{\partial \mathcal{H}}{\partial \mathbf{S}_i} \right\rangle = -\frac{1}{\mathcal{Z}_c} \text{Tr}_c \left(e^{-\beta \mathcal{H}} \frac{\partial \mathcal{H}}{\partial \mathbf{S}_i} \right). \quad (\text{A13})$$

From the explicit form of the DE Hamiltonian in Eq. (1), we can further simplify the expression Eq. (A13) (note: repeated greek indices imply summation over spins)

$$\mathbf{T}_i(t) = J \boldsymbol{\sigma}_{\alpha\beta} \rho_{i\beta, i\alpha}^*(t), \quad (\text{A14})$$

where we have introduced the quasiequilibrium one-electron correlation function or density matrix

$$\rho_{i\alpha, j\beta}^*(t) \equiv \langle \hat{c}_{j\beta}^\dagger \hat{c}_{i\alpha} \rangle = \frac{1}{\mathcal{Z}_c} \text{Tr}_c(e^{-\beta \mathcal{H}(\{\mathbf{S}_i(t)\})} \hat{c}_{j\beta}^\dagger \hat{c}_{i\alpha}). \quad (\text{A15})$$

The density matrix can be straightforwardly computed from the eigenvalues and eigenvectors of the Hamiltonian matrix Eq. (11). However, exact diagonalization for $\rho_{i\alpha, j\beta}^*$ is not feasible for large-scale simulations, since its computational time scales cubically with the system size. Linear-scaling method

for the calculation of density matrix can be achieved using, e.g., the kernel polynomial method (KPM) or recent machine learning techniques.

2. Nonadiabatic Ehrenfest dynamics of double-exchange systems

For nonadiabatic dynamics of the DE system, both electrons and spins evolve with time according to their respective governing dynamical equations. We first consider the case in which the electrons are in a pure state described by an instantaneous many-electron wave function $|\Psi(t)\rangle$. The evolution of this wave function is governed by the Schrödinger equation

$$i\hbar \frac{d|\Psi\rangle}{dt} = \mathcal{H}(\{\mathbf{S}_i(t)\}) |\Psi\rangle. \quad (\text{A16})$$

Here \mathcal{H} is the DE Hamiltonian Eq. (1), which depends on time through the spins. To describe the spin dynamics, one then defines an effective energy $\mathcal{E}(\Psi) \equiv \langle \Psi | \mathcal{H} | \Psi \rangle$, which is the energy corresponding to the electron wave function $|\Psi\rangle$. The torques acting on spins are, again, given by the Hellmann-Feynman formula

$$\mathbf{T}_i = -\frac{\partial \langle \Psi | \mathcal{H} | \Psi \rangle}{\partial \mathbf{S}_i} = -\langle \Psi | \frac{\partial \mathcal{H}}{\partial \mathbf{S}_i} | \Psi \rangle. \quad (\text{A17})$$

Here we have neglected the derivatives $\partial|\Psi\rangle/\partial\mathbf{S}_i$ since the electron wave function $|\Psi\rangle$ does not explicitly depend on spins. Instead, as described above in Eq. (A16), the electrons coupled to spins through a time-dependent Hamiltonian. For a closed DE system, the energy conserving spin dynamics is described by the Landau-Lifshitz equation, which is given by Eq. (A9) with $\alpha = 0$:

$$\frac{d\mathbf{S}_i}{dt} = \mathbf{S}_i \times \langle \Psi | \frac{\partial \mathcal{H}}{\partial \mathbf{S}_i} | \Psi \rangle = -J\mathbf{S}_i \times \boldsymbol{\sigma}_{\alpha\beta} \langle \Psi(t) | \hat{c}_{i\alpha}^\dagger \hat{c}_{i\beta} | \Psi(t) \rangle. \quad (\text{A18})$$

These two coupled equations (A16) and (A18) offer a complete description of the nonadiabatic dynamics for closed DE-type systems [60,61,76], similar to the Ehrenfest dynamics for quantum MD simulations [40].

Importantly, since the DE Hamiltonian is bilinear in fermion operators, the many-electron wave function $|\Psi(t)\rangle$ is a time-dependent single Slater determinant state [77]

$$|\Psi(t)\rangle = \prod_{m=1}^{N_e} \hat{\psi}_m^\dagger(t) |0\rangle, \quad (\text{A19})$$

where the time-varying quasiparticle operators satisfy the Heisenberg equation of motion

$$\frac{d\hat{\psi}_m}{dt} = \frac{i}{\hbar} [\hat{\mathcal{H}}(\{\mathbf{S}_i(t)\}), \hat{\psi}_m(t)] \quad (\text{A20})$$

and are subject to an initial condition such that $\{\hat{\psi}_m^\dagger(0)\}$ diagonalize the DE Hamiltonian at $t = 0$, i.e.,

$$\hat{\mathcal{H}}(\{\mathbf{S}_i(0)\}) = \sum_m \varepsilon_m \hat{\psi}_m^\dagger(0) \hat{\psi}_m(0). \quad (\text{A21})$$

However, the numerical integration of the Slater determinant is rather cumbersome. So far, this method has been applied to study the photoinduced dynamics of rather small lattices [60,61,76].

3. Landau-Lifshitz-von Neumann dynamics for DE systems

An alternative formulation of the nonadiabatic Ehrenfest dynamics is based on the single-particle density matrix. This approach also allows for inclusion of correlations in the initial state in the nonadiabatic electron dynamics. To this end, we switch to the Heisenberg picture and consider time-dependent operators. We define an effective energy functional

$$\mathcal{E}(\{\mathbf{S}_i\}) \equiv \text{Tr}[\hat{\rho}^{(0)} \hat{\mathcal{H}}(\{\mathbf{S}_i\})] \equiv \sum_\lambda P_\lambda \langle \Phi_\lambda | \hat{\mathcal{H}}(\{\mathbf{S}_i\}) | \Phi_\lambda \rangle. \quad (\text{A22})$$

Here $\hat{\rho}^{(0)} = \sum_\lambda P_\lambda |\Phi_\lambda\rangle \langle \Phi_\lambda|$ denotes an initial many-electron density matrix, and $\{|\Phi_\lambda\rangle\}$ form an ensemble of initial many-electron state. For the case of pure state, $\hat{\rho}^{(0)} = |\Phi\rangle \langle \Phi|$, and when $|\Phi\rangle$ is given by the ground state $|\Psi\rangle$, this energy is reduced to the case discussed above. For application to elementary excitations of a finite-temperature thermal state, we take $|\Phi_\lambda\rangle$ to be the many-electron eigenstates of the Hamiltonian at $t = 0$ and $P_\lambda \propto e^{-\beta \varepsilon_\lambda}$ to be the Boltzmann distribution.

Given this energy functional, the torques acting on spins are computed as

$$\mathbf{T}_i(t) = -\frac{\partial \text{Tr}(\hat{\rho}^{(0)} \hat{\mathcal{H}})}{\partial \mathbf{S}_i} = -\text{Tr}\left(\hat{\rho}^{(0)} \frac{\partial \hat{\mathcal{H}}}{\partial \mathbf{S}_i}\right) = J\boldsymbol{\sigma}_{\alpha\beta} \rho_{i\beta, i\alpha}(t). \quad (\text{A23})$$

Note that repeated greek indices imply summation over spins. Here we have also invoked the general Hellmann-Feynman theorem for the second identity. In the third equality, we have used the explicit form of the Hund's rule coupling in DE Hamiltonian (1) and introduced the time-dependent single-electron density matrix

$$\rho_{i\alpha, j\beta}(t) \equiv \text{Tr}[\hat{\rho}^{(0)} \hat{c}_{j\beta}^\dagger(t) \hat{c}_{i\alpha}(t)]. \quad (\text{A24})$$

Substituting Eq. (A23) into the Landau-Lifshitz equation (A9) and setting $\alpha = 0$, we obtain

$$\frac{d\mathbf{S}_i}{dt} = -J\mathbf{S}_i \times \boldsymbol{\sigma}_{\alpha\beta} \rho_{i\beta, i\alpha}(t). \quad (\text{A25})$$

This spin dynamics equation has to be supplemented by the equation of motion for the density matrix $\rho_{i\alpha, j\beta}$, which can be obtained using the Heisenberg equation for the electron or fermion operators, e.g.,

$$\frac{d\hat{c}_{i\alpha}}{dt} = \frac{1}{i\hbar} [\hat{c}_{i\alpha}, \hat{\mathcal{H}}] = \frac{1}{i\hbar} H_{i\alpha, j\beta} \hat{c}_{j\beta}. \quad (\text{A26})$$

The resultant equation is the von Neumann equation with the one-particle Hamiltonian matrix $H_{i\alpha, j\beta}$, i.e., $d\rho/dt = [H, \rho]/i\hbar$, or explicitly

$$\begin{aligned} \frac{d\rho_{i\alpha, j\beta}}{dt} &= i \sum_k (t_{ik} \rho_{k\alpha, j\beta} - \rho_{i\alpha, k\beta} t_{kj}) \\ &+ iJ(\mathbf{S}_i \cdot \boldsymbol{\sigma}_{\alpha\gamma} \rho_{i\gamma, j\beta} - \rho_{i\alpha, j\gamma} \boldsymbol{\sigma}_{\gamma\beta} \cdot \mathbf{S}_j). \end{aligned} \quad (\text{A27})$$

The coupled ordinary differential equations (A25) and (A27), called the Landau-Lifshitz-von Neumann dynamics, offer a complete description for the evolution of the DE system. Numerically, thanks to the sparsity of the Hamiltonian matrix, the von Neumann Eq. (A27) can be efficiently integrated using sparse matrix multiplication algorithms.

- [1] M. Seul and D. Andelman, Domain shapes and patterns: The phenomenology of modulated phases, *Science* **267**, 476 (1995).
- [2] J. P. Gollub and J. S. Langer, Pattern formation in nonequilibrium physics, *Rev. Mod. Phys.* **71**, S396 (1999).
- [3] J. D. Gunton, M. San Miguel, and P. S. Saint, The dynamics of first order phase transitions, in *Phase Transitions and Critical Phenomena*, edited by C. Domb and J. L. Lebowitz, Vol. 8 (Academic, New York, 1983), pp. 269–466.
- [4] E. Dagotto, Complexity in strongly correlated electronic systems, *Science* **309**, 257 (2005).
- [5] S. A. Kivelson, E. Fradkin, and V. J. Emery, Electronic liquid-crystal phases of a doped Mott insulator, *Nature (London)* **393**, 550 (1998).
- [6] S. A. Kivelson, I. P. Bindloss, E. Fradkin, V. Oganesyan, J. M. Tranquada, A. Kapitulnik, and C. Howald, How to detect fluctuating stripes in the high-temperature superconductors, *Rev. Mod. Phys.* **75**, 1201 (2003).
- [7] A. Moreo, S. Yunoki, and E. Dagotto, Phase separation scenario for manganese oxides and related materials, *Science* **283**, 2034 (1999).
- [8] E. Dagotto, T. Hotta, and A. Moreo, Colossal magnetoresistant materials: The key role of phase separation, *Phys. Rep.* **344**, 1 (2001).
- [9] N. Mathur and P. Littlewood, Mesoscopic texture in manganites, *Phys. Today* **56**(1), 25 (2003).
- [10] E. Dagotto, *Nanoscale Phase Separation And Colossal Magnetoresistance* (Springer, Berlin, 2002).
- [11] M. B. Salamon and M. Jaime, The physics of manganites: Structure and transport, *Rev. Mod. Phys.* **73**, 583 (2001).
- [12] M. Fäth, S. Freisem, A. A. Menovsky, Y. Tomioka, J. Aarts, and J. A. Mydosh, Spatially inhomogeneous metal-insulator transition in doped manganites, *Science* **285**, 1540 (1999).
- [13] C. Renner, G. Aeppli, B.-G. Kim, Y.-A. Soh, and S.-W. Cheong, Atomic-scale images of charge ordering in mixed-valance manganite, *Nature (London)* **416**, 518 (2002).
- [14] L. Zhang, C. Israel, A. Biswas, R. L. Greene, A. de Lozanne, Direct observation of percolation in a manganite thin film, *Science* **298**, 805 (2002).
- [15] M. Uehara, S. Mori, C. H. Chen, and S.-W. Cheong, Percolative phase separation underlies colossal magnetoresistance in mixed-valent manganites, *Nature (London)* **399**, 560 (1999).
- [16] P. Schiffer, A. P. Ramirez, W. Bao, and S.-W. Cheong, Low Temperature Magnetoresistance and the Magnetic Phase Diagram of $\text{La}_{1-x}\text{Ca}_x\text{MnO}_3$, *Phys. Rev. Lett.* **75**, 3336 (1995).
- [17] J. Burgy, M. Mayr, V. Martin-Mayor, A. Moreo, and E. Dagotto, Colossal Effects in Transition Metal Oxide Caused by Intrinsic Inhomogeneities, *Phys. Rev. Lett.* **87**, 277202 (2001).
- [18] C. Zener, Interaction between the d -Shells in the Transition Metals. II. Ferromagnetic Compounds of Manganese with Perovskite Structure, *Phys. Rev.* **82**, 403 (1951).
- [19] P. W. Anderson and H. Hasegawa, Considerations on Double Exchange, *Phys. Rev.* **100**, 675 (1955).
- [20] P.-G. de Gennes, Effects of double exchange in magnetic crystals, *Phys. Rev.* **118**, 141 (1960).
- [21] J. Zhang, F. Ye, H. Sha, P. Dai, J. A. Fernandez-Baca, and E. W. Plummer, Magnons in ferromagnetic metallic manganites, *J. Phys.: Cond. Matter* **19**, 315204 (2007).
- [22] H. Y. Hwang, P. Dai, S.-W. Cheong, G. Aeppli, D. A. Tennant, and H. A. Mook, Softening and Broadening of the Zone Boundary Magnons in $\text{Pr}_{0.63}\text{Sr}_{0.37}\text{MnO}_3$, *Phys. Rev. Lett.* **80**, 1316 (1998).
- [23] J. A. Fernandez-Baca, P. Dai, H. Y. Hwang, C. Kloc, and S.-W. Cheong, Evolution of the Low-Frequency Spin Dynamics in Ferromagnetic Manganites, *Phys. Rev. Lett.* **80**, 4012 (1998).
- [24] P. Dai, H. Y. Hwang, J. Zhang, J. A. Fernandez-Baca, S.-W. Cheong, C. Kloc, Y. Tomioka, and Y. Tokura, Magnon damping by magnon-phonon coupling in manganese perovskites, *Phys. Rev. B* **61**, 9553 (2000).
- [25] F. Ye, P. Dai, J. A. Fernandez-Baca, H. Sha, J. W. Lynn, H. Kawano-Furukawa, Y. Tomioka, Y. Tokura, and J. Zhang, Evolution of Spin-Wave Excitations in Ferromagnetic Metallic Manganites, *Phys. Rev. Lett.* **96**, 047204 (2006).
- [26] J. S. Helton, S. K. Jones, D. Parshall, M. B. Stone, D. A. Shulyatev, and J. W. Lynn, Spin wave damping arising from phase coexistence below T_c in colossal magnetoresistive $\text{La}_{0.7}\text{Ca}_{0.3}\text{MnO}_3$, *Phys. Rev. B* **96**, 104417 (2017).
- [27] N. Furukawa, Spin Excitation Spectrum of $\text{La}_{1-x}\text{A}_x\text{MnO}_3$, *J. Phys. Soc. Jpn.* **65**, 1174 (1996).
- [28] Y. Motome, N. Furukawa, Monte Carlo study of doping change and disorder effect on double-exchange ferromagnetism, *Phys. Rev. B* **68**, 144432 (2003).
- [29] D. I. Golosov, Spin Wave Theory of Double Exchange Ferromagnets, *Phys. Rev. Lett.* **84**, 3974 (2000).
- [30] N. Shannon and A. V. Chubukov, Spin-wave expansion, finite temperature corrections, and order from disorder effects in the double exchange model, *Phys. Rev. B* **65**, 104418 (2002).
- [31] M. D. Kapetanakis and I. E. Perakis, Non-Heisenberg spin dynamics of double-exchange ferromagnets with Coulomb repulsion, *Phys. Rev. B* **75**, 140401(R) (2007).
- [32] N. Furukawa, Magnon linewidth broadening due to magnon-phonon interactions in colossal magnetoresistance manganites, *J. Phys. Soc. Jpn.* **68**, 2522 (1999).
- [33] L. M. Woods, Magnon-phonon effects in ferromagnetic manganites, *Phys. Rev. B* **65**, 014409 (2001).
- [34] S. Krivenko, A. Yaresko, G. Khaliullin, and H. Fehske, Magnon softening and damping in the ferromagnetic manganites due to orbital correlations, *J. Magn. Magn. Mater.* **272–276**, 458 (2004).
- [35] Y. Motome and N. Furukawa, Disorder effect on spin excitation in double-exchange systems, *Phys. Rev. B* **71**, 014446 (2005).
- [36] E. C. Andrade and M. Vojta, Disorder, Cluster Spin Glass, and Hourglass Spectra in Striped Magnetic Insulators, *Phys. Rev. Lett.* **109**, 147201 (2012).
- [37] Y. Drees, Z. W. Li, A. Ricci, M. Rotter, W. Schmidt, D. Lamago, O. Sobolev, U. Rütt, O. Gutowski, M. Sprung, A. Piovano, J. P. Castellan, and A. C. Komarek, Hour-glass magnetic excitations induced by nanoscopic phase separation in cobalt oxides, *Nat. Commun.* **5**, 5731 (2014).
- [38] S. Bhattacharyya, S. S. Bakshi, S. Kadge, and P. Majumdar, Langevin approach to lattice dynamics in a charge-ordered polaronic system, *Phys. Rev. B* **99**, 165150 (2019).
- [39] S. Bhattacharyya, S. S. Bakshi, S. Pradhan, and P. Majumdar, Strongly anharmonic collective modes in a coupled electron-phonon-spin problem, *Phys. Rev. B* **101**, 125130 (2020).
- [40] D. Marx and J. Hutter, *Ab Initio Molecular Dynamics: Basic Theory And Advanced Methods* (Cambridge University Press, Cambridge, 2009).

- [41] G.-W. Chern, K. Barros, Z. Wang, H. Suwa, and C. D. Batista, Semiclassical dynamics of spin density waves, *Phys. Rev. B* **97**, 035120 (2018).
- [42] S. Yunoki, J. Hu, A. L. Malvezzi, A. Moreo, N. Furukawa, and E. Dagotto, Phase Separation in Electronic Models for Manganites, *Phys. Rev. Lett.* **80**, 845 (1998).
- [43] E. Dagotto, S. Yunoki, A. L. Malvezzi, A. Moreo, J. Hu, S. Capponi, D. Poilblanc, and N. Furukawa, Ferromagnetic Kondo model for manganites: Phase diagram, charge segregation, and influence of quantum localized spins, *Phys. Rev. B* **58**, 6414 (1998).
- [44] A. Chattopadhyay, A. J. Millis, and S. Das Sarma, $T = 0$ phase diagram of the double-exchange model, *Phys. Rev. B* **64**, 012416 (2001).
- [45] M. Azhar and M. Mostovoy, Incommensurate Spiral Order from Double-Exchange Interactions, *Phys. Rev. Lett.* **118**, 027203 (2017).
- [46] N. Furukawa and Y. Motome, Order N Monte Carlo algorithm for fermion systems coupled with fluctuating adiabatic fields, *J. Phys. Soc. Jpn.* **73**, 1482 (2004).
- [47] G. Alvarez, C. Sen, N. Furukawa, Y. Motome, and E. Dagotto, The truncated polynomial expansion Monte Carlo method for fermion systems coupled to classical fields: A model independent implementation, *Comput. Phys. Commun.* **168**, 32 (2005).
- [48] A. Weisse, G. Wellein, A. Alvermann, and H. Fehske, The kernel polynomial method, *Rev. Mod. Phys.* **78**, 275 (2006).
- [49] K. Barros and Y. Kato, Efficient Langevin simulation of coupled classical fields and fermions, *Phys. Rev. B* **88**, 235101 (2013).
- [50] K. Barros, J. W. F. Venderbos, G.-W. Chern, and C. D. Batista, Exotic magnetic orderings in the kagome Kondo-lattice model, *Phys. Rev. B* **90**, 245119 (2014).
- [51] Z. Wang, G.-W. Chern, C. D. Batista, and K. Barros, Gradient-based stochastic estimation of the density matrix, *J. Chem. Phys.* **148**, 094107 (2018).
- [52] P. C. Hohenberg and B. I. Halperin, Theory of dynamic critical phenomena, *Rev. Mod. Phys.* **49**, 435 (1977).
- [53] Q. Niu, X. Wang, L. Kleinman, W.-M. Liu, D. M. C. Nicholson, and G. M. Stocks, Adiabatic Dynamics of Local Spin Moments in Itinerant Magnets, *Phys. Rev. Lett.* **83**, 207 (1999).
- [54] K. Capelle, G. Vignale, and B. L. Györfy, Spin Currents and Spin Dynamics in Time-Dependent Density-Functional Theory, *Phys. Rev. Lett.* **87**, 206403 (2001).
- [55] Z. Qian and G. Vignale, Spin Dynamics from Time-Dependent Spin-Density-Functional Theory, *Phys. Rev. Lett.* **88**, 056404 (2002).
- [56] J. C. Tully, Molecular dynamics with electronic transitions, *J. Chem. Phys.* **93**, 1061 (1990).
- [57] X. Li, J. C. Tully, H. B. Schlegel, and M. J. Frisch, *Ab initio* Ehrenfest dynamics, *J. Chem. Phys.* **123**, 084106 (2005).
- [58] P. Fazekas, *Lecture Notes on Electron Correlation and Magnetism* (World Scientific Publishing, Singapore, 1999).
- [59] P.-W. Ma and S. L. Dudarev, Longitudinal magnetic fluctuations in Langevin spin dynamics, *Phys. Rev. B* **86**, 054416 (2012).
- [60] W. Koshibae, N. Furukawa, and N. Nagaosa, Photo-induced insulator-metal transition of a spin-electron coupled system, *Europhys. Lett.* **94**, 27003 (2011).
- [61] A. Ono and S. Ishihara, Double-Exchange Interaction in Optically Induced Nonequilibrium State: A Conversion from Ferromagnetic to Antiferromagnetic Structure, *Phys. Rev. Lett.* **119**, 207202 (2017).
- [62] N. Furukawa, Transport properties of the Kondo lattice model in the limit $S = \infty$ and $D = \infty$, *J. Phys. Soc. Jpn.* **63**, 3214 (1994).
- [63] C. M. Varma, Electronic and magnetic states in the giant magnetoresistive compounds, *Phys. Rev. B* **54**, 7328 (1996).
- [64] J. M. D. Coey, M. Viret, L. Ranno, and K. Ounadjela, Electron Localization in Mixed-Valence Manganites, *Phys. Rev. Lett.* **75**, 3910 (1995).
- [65] H. Yi, N. H. Hur, and J. Yu, Anomalous spin susceptibility and magnetic polaron formation in the double-exchange systems, *Phys. Rev. B* **61**, 9501 (2000).
- [66] A. Chakraborty and G. Bouzerar, Dynamical properties of a three-dimensional diluted Heisenberg model, *Phys. Rev. B* **81**, 172406 (2010).
- [67] M. Vojta, Excitation Spectra of Disordered Dimer Magnets Near Quantum Criticality, *Phys. Rev. Lett.* **111**, 097202 (2013).
- [68] D. Stauffer and A. Aharony, *Introduction to Percolation Theory*, Revised second edition (Taylor & Francis Inc, Philadelphia, 1994).
- [69] Here we have used $\tau = 187/91 \approx 2.054$ from the 2D percolation theory.
- [70] T. Chatterji, M. M. Koza, F. Demmel, W. Schmidt, J.-U. Hoffmann, U. Aman, R. Schneider, G. Dhalenne, R. Suryanarayanan, and A. Revcolevschi, Coexistence of ferromagnetic and antiferromagnetic spin correlation in $\text{La}_{1.2}\text{Sr}_{1.8}\text{Mn}_2\text{O}_7$, *Phys. Rev. B* **73**, 104449 (2006).
- [71] W. F. Brown, Jr., Thermal fluctuations of a single-domain particle, *Phys. Rev.* **130**, 1677 (1963).
- [72] V. P. Antropov, S. V. Tretyakov, and B. N. Harmon, Spin dynamics in magnets: Quantum effects and numerical simulations, *J. Appl. Phys.* **81**, 3961 (1997).
- [73] P.-W. Ma and S. L. Dudarev, Langevin spin dynamics, *Phys. Rev. B* **83**, 134418 (2011).
- [74] M. Weinert and J. W. Davenport, Fractional occupations and density-functional energies and forces, *Phys. Rev. B* **45**, 13709 (1992).
- [75] R. M. Wentzcovitch, J. L. Martins, and P. B. Allen, Energy versus free-energy conservation in first-principles molecular dynamics, *Phys. Rev. B* **45**, 11372 (1992).
- [76] W. Koshibae, N. Furukawa, and N. Nagaosa, Real-Time Quantum Dynamics of Interacting Electrons: Self-Organized Nanoscale Structure in a Spin-Electron Coupled System, *Phys. Rev. Lett.* **103**, 266402 (2009).
- [77] M. Imada and Y. Hatsugai, Numerical studies on the hubbard model and the t - J model in one- and two-dimensions, *J. Phys. Soc. Jpn.* **58**, 3752 (1989).